On the Implementation of Variable Speed in Pump-Turbine Units Providing Primary and Secondary Load-Frequency Control in Generating Mode

José Ignacio Sarasúa *,†, Juan Ignacio Pérez-Díaz † and Blanca Torres Vara

Department of Hydraulic, Energy and Environmental Engineering, School of Civil Engineering,
Technical University of Madrid, C/Profesor Aranguren, Madrid 28040, Spain; ji.perez@upm.es (J.I.P.-D.);
blancatorresvara@gmail.com (B.T.V.)
* Correspondence: joseignacio.sarasua@upm.es; Tel.: +34-91-336-6705; Fax: +34-91-336-6764
† These authors contributed equally to this work.

Abstract: This paper analyses different control strategies for the speed control loop of a variable-speed pump-turbine unit equipped with a doubly fed induction generator, operating in generating mode in an isolated power system with high penetration of intermittent renewable energy. The control strategies are evaluated and compared to each other in terms of the amount of water discharged through the pump-turbine and of the wicket gates fatigue while providing primary and secondary load-frequency control. The influence of the penstock length and the initial operating point on the performance of each control strategy is studied in detail. For these purposes, several simulations have been performed with a suitable dynamic model of the pumped-storage hydropower plant and the power system. The results of the paper indicate that a proper control strategy would consist in updating the reference speed according to the power generation schedule and keeping it constant within each scheduling period (typically 1 h).

Keywords: pumped storage hydropower plant (PSHP); variable speed operation; load-frequency control

1. Introduction

The integration of intermittent energy sources in the grid is one of the most important challenges for hydropower plants nowadays [1]. Excess wind and solar energy is a real fact, especially in isolated systems, such as small or medium size island electric power systems [2]. The penetration of these intermittent sources is very high in order to avoid environmental and social costs of fossil fuel-based electricity generation [3,4]. Pumped storage hydropower plants (PSHPs) are useful to hedge against the uncertainty in intermittent renewable energy (wind and solar) [5]. PSHPs can contribute significantly to the load-frequency control in generating mode. In pumping mode, variable-speed or hydraulic short-circuit operation is required to provide load-frequency control [6,7].

Doubly fed induction generators (DFIG) are widely used for variable speed pumped-storage units [8,9]. In [10] two control schemes are proposed for variable speed pumped-storage units operating in generating mode. In the load control scheme, the power injected into the grid is regulated by the rotor-side converter and the turbine governor is in charge of restoring the unit running speed to the reference value. In this way, the electric power delivered by the unit is free from water hammer effects since the variations in the turbine mechanical power are absorbed by the inertia of the

rotational masses. In addition, the reference speed can be modified in a speed control loop in order to increase the hydraulic efficiency [11].

The dynamic response of a PSHP equipped with a DFIG and load control scheme has been analyzed in detail in [12–14]. In [12,13] the speed reference is kept constant during the simulations, whereas in [14] only a sudden decrease of the active power set point is simulated. There are therefore several questions regarding the speed control loop which have not been answered yet. Variable speed pumped-storage units are expected to provide primary and secondary load-frequency control both in generating and pumping mode. As it is well known, variable speed allows increasing the efficiency in turbine mode. However, to authors' knowledge there is no previous work on how to update the reference speed of a hydropower unit when it provides load-frequency control, as most hydropower units do. How often the optimal speed (as referred to in [14]) should be updated in order to provide primary and secondary load-frequency control in an optimum way is the main question addressed in this paper. In order to ask this question, it is necessary to define a criterion to evaluate the performance of the pump-turbine unit. The criterion used in this paper for this purpose is based on the amount of water discharged through the pump-turbine, and on the fatigue of the wicket gates servo mechanism, while providing load-frequency control: the lower the water usage (and therefore the necessary energy consumption for pumping) and the wicket gates fatigue, the better the pump-turbine performance, provided that the response meets certain quality standards.

This paper studies and compares to each other different control strategies for the speed control loop of a PSHP equipped with a pump-turbine and a DFIG when it operates in generating mode. The PSHP is connected to a small isolated power system with thermal, wind and solar generation, and which provides secondary load-frequency control under the orders of an automatic generation control (AGC) system.

A dynamic model of the PSHP and the power system has been developed and several simulations have been carried out in order to evaluate and compare to each other the proposed control strategies. Moreover, the influence of the initial operating point (initial power and gross head) and the penstock length on the performance of each control strategy has been analyzed in detail.

The remainder of the paper is organized as follows: in Section 2, the main characteristics of the PSHP and the power system where the study is carried out are presented; in Section 3 the non-linear dynamic model of the considered power system is described; the control strategies formulated for the speed control loop are described in Section 4; the simulations carried out in this study are described in Section 5; the results of the simulations are presented in Section 6; finally, the main conclusions of the paper are summarized in Section 7.

2. Description of the Pumped Storage Hydropower Plant and the Power System

The PSHP modelled in this paper is equipped with a pump-turbine unit coupled to a DFIG and the rated power of the unit is 14.97 MW. Two solutions with different penstock length (1350-m and 300-m) have been studied in order to gain insight on the influence of the conduit water inertia on the dynamic response of the PSHP. There is no surge tank in the scheme and the tail race tunnel is not considered due to its short length. The power system to which the PSHP is connected comprises six fuel-oil generating units, five diesel-oil generating units, seven gas-oil generating units and two combined cycle gas units. The total installed thermal generation power in July 2012 was 852 MW [7]; in addition, there were 35 MW and 24 MW of wind and photovoltaic generation at that time.

3. Dynamic Model

Figure 1 shows the block diagram of the simulation model developed in Matlab-Simulink. Each block of the diagram is briefly described below.

3.1. Penstock

Hydraulic transients in close conduits are properly described by a couple of partial differential equations, usually referred to as mass and momentum conservation equations [15]. In this paper, a lumped parameters model has been used to transform the above-mentioned system of partial differential equations in a system of ordinary differential equations [13,16]. For the long penstock configuration, the penstock has been modelled through Equations (1) and (2), considering ten Γ-shaped consecutive elements ($n_{ge} = 10$), Figure 2 [7,17].
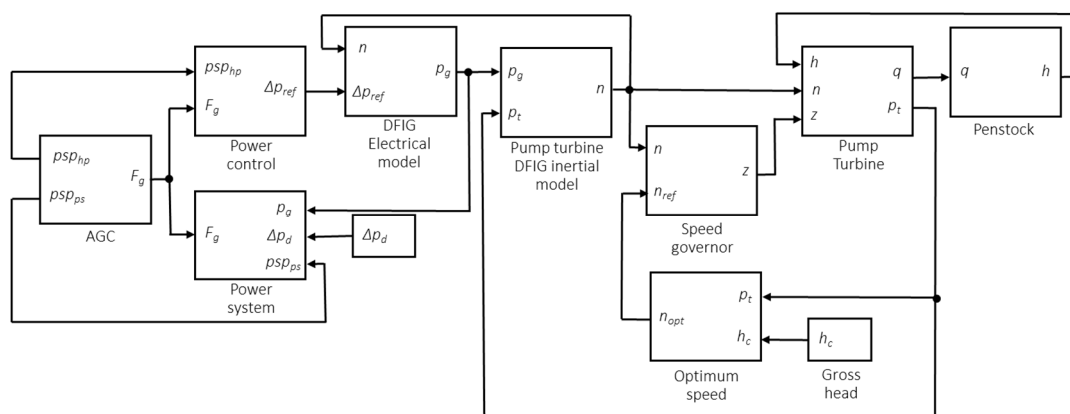

Figure 1. Block diagram of the dynamic model. All variables are expressed in p.u. values with respect to the base values included in Table 1.

Table 1. Model base values.

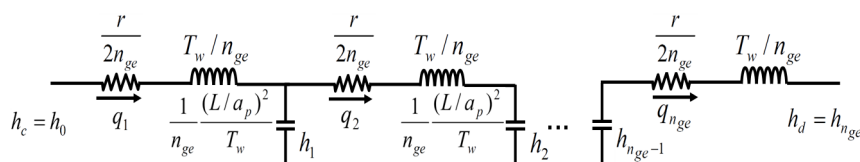| Parameter	Value	Parameter	Value
Q_b	10 m^3/s	P_b (base power)	14.93 MW
H_b	165.19 m	F_b (base frequency)	50 Hz
N_b (base running speed)	600 r.p.m	D (turbine diameter)	1.31 m

Figure 2. Scheme of the long penstock model.

$$\frac{\mathrm{d}q_i}{\mathrm{d}t} = \frac{n_{ge}}{T_w}\left(h_{i-1} - h_i - \frac{r}{2n_{ge}}q_i^2\right) \text{ and } T_w = \frac{L}{gF}\frac{Q_b}{H_b} \tag{1}$$

$$\frac{\mathrm{d}h_i}{\mathrm{d}t} = \frac{T_w n_{ge}}{T_e^2}\left(q_i - q_{i+1}\right) \text{ and } T_e = \frac{L}{a_p} \tag{2}$$

In Equations (1) and (2), n_{ge} is the number of elements, h_i (p.u.) is the head at the end of the i-th Γ element, q_i (p.u.) is the flow in the i-th Γ element, T_w (s) is the water starting time, L (m) is the penstock length, g (m/s^2) is the gravity acceleration, F (m^2) is the penstock cross section, Q_b (m^3/s) is base flow, H_b (m) is the base head, T_e (s) is the water elastic time, a_p (m/s) is the penstock wave speed and r (p.u.) is twice the head loss in the penstock with rated flow.

For the short penstock configuration, the penstock has been modelled through Equations (3) and (4), considering a single Π-shaped element, Figure 3. The element has one series branch and two shunt branches. The total head losses are included in the series branch of Equation (3), whereas

the elasticity effects are included in the shunt branches of Equation (4). Expression in Equation (4) includes a correction coefficient β to match the first peak of the frequency response of the continuous model [18].
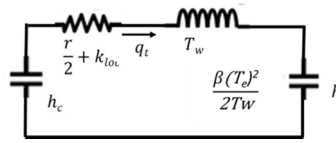

Figure 3. Scheme of the short penstock model.

$$\frac{\mathrm{d}q_t}{\mathrm{d}t} = \frac{1}{T_\mathrm{w}}\left(h_\mathrm{c} - h - \frac{r}{2}q_\mathrm{t}\,|q_\mathrm{t}|\right) \tag{3}$$

$$\frac{\mathrm{d}h}{\mathrm{d}t} = \frac{2T_\mathrm{w}}{\beta T_\mathrm{e}^2}\left(q_\mathrm{t} - q\right) \text{ where } \beta = \frac{8}{\pi^2} \tag{4}$$

In Equations (3) and (4), h_c is the gross head, h is the net head at the pump-turbine inlet, q_t is the flow in the penstock, and q is the flow through the pump-turbine.

3.2. Pump-Turbine

The performance curves of the pump-turbine unit in generating mode have been approximated by those used in [17] and are shown in Figure 4. In this case the hill chart, expressed as a function of the unit speed n_{11} and flow q_{11} in Equation (5), is experimental, where z is the wicket gates position. In the absence of experimental data, the selection of the pump-turbine model can be crucial to accurately predict its behavior with variable speed [19].
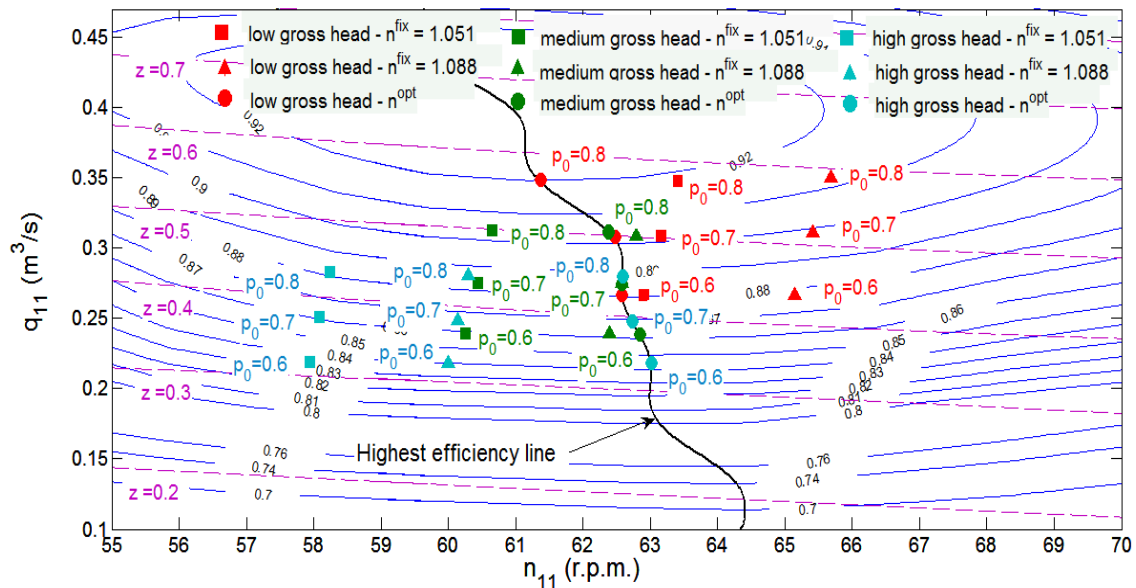
Figure 4. Pump-turbine performance curves in generating mode; considered initial operating points superimposed in the curves.

The "pump-turbine" block calculates the flow discharged through the pump-turbine runner q, as well as the shaft mechanical power p_t, by interpolating in the above-mentioned performance curves. Turbine dynamics has been neglected.

$$n_{11} = \frac{nD}{\sqrt{H}} \quad q_{11} = \frac{q}{D^2\sqrt{H}} \tag{5}$$

3.3. Optimal Speed

The "optimal speed" block determines the optimal running speed of the unit for a given mechanical power p_t and gross head h_c, by interpolating iteratively in the pump-turbine performance curves. The optimal running speed is defined as the one which allows generating the given mechanical power with the highest efficiency, or rather, with the lowest water discharge. The block searches for the optimal speed within the pump-turbine hill chart, which have been previously parameterized.

3.4. Pump-Turbine-Doubly Fed Induction Generator Inertial Model

The "pump-turbine-DFIG inertial model" block calculates the unit running speed n from the unbalance between the electrical power delivered to the grid p_g and the shaft mechanical power p_t in Equation (6):

$$T_m \cdot \frac{dn}{dt} \cdot n = p_t - p_g \tag{6}$$

T_m (s) is the mechanical starting time of the unit.

3.5. Speed Governor

The control diagram proposed in [10] for the speed governor of a hydro unit with DFIG is used in the present work. The "optimal speed" block sends the reference speed n^{ref} to the "speed governor" block and a conventional PI controller in Equation (7) acts on the wicket gates opening z in order to follow the optimal speed signal:

$$\frac{d\Delta z}{dt} = \frac{1}{\delta}\frac{d(n^{ref} - n)}{dt} + \frac{(n^{ref} - n)}{\delta T_r} \tag{7}$$

The controller gains are expressed in terms of the parameters used to model the classical mechanical hydraulic governor, δ is transient speed drop, and T_r (s) is dashpot time constant. Two different pairs of controller gains have been used depending on the penstock length.

3.6. Power Control

The changes in the electrical power required to the DFIG Δp_{ref} in Equation (8), are calculated from the variations in the power set-point signal sent by the AGC system psp_{hp} (p.u.), and the system frequency deviation F_g (rd/s), in the "power control" block. The variations in the pump-turbine power set-point due to the contribution of the PSHP to the primary load-frequency control p_{R1} (p.u.), has been modelled in a similar way to [20] in Equation (9). Two different control actions are considered: a droop-based control action p_{R1E} (p.u.) in Equation (10), and an inertia emulation control action p_{R1I} (p.u.) in Equation (11), [21,22]:

$$\Delta p_{ref} = -p_{R1} + psp_{hp} \tag{8}$$

$$p_{R1} = p_{R1E} + p_{R1I} \tag{9}$$

$$p_{R1E} = K \cdot \frac{F_g}{\omega^0} \tag{10}$$

$$T_{fnf}\frac{dp_{R1I}}{dt} + p_{R1I} = T_d \frac{dF_g}{dt} \tag{11}$$

In expression of Equation (10), ω^0 (rd/s) is the base system frequency. In expression of Equation (11) T_d (s) is the derivative gain and T_{fnf} (s) is the time constant of the Power control block.

3.7. Doubly Fed Induction Generator Electrical Model

The electromagnetic torque is assumed to be controlled by the rotor-side inverter [23,24] in an instantaneous manner, comparing to the dynamics studied in the paper. In the "DFIG electrical model" block the electromagnetic torque, c_{em} (p.u.) and the rotor power, p_r (p.u.) are calculated from the running speed, n and the required electric power, $(p^0 + \Delta p_{ref})$ (Figure 5). If none of these values exceeds its corresponding upper limit, the electric power output matches exactly the required electric power; otherwise, the electric power output is conveniently limited. The power losses in the generator are neglected.
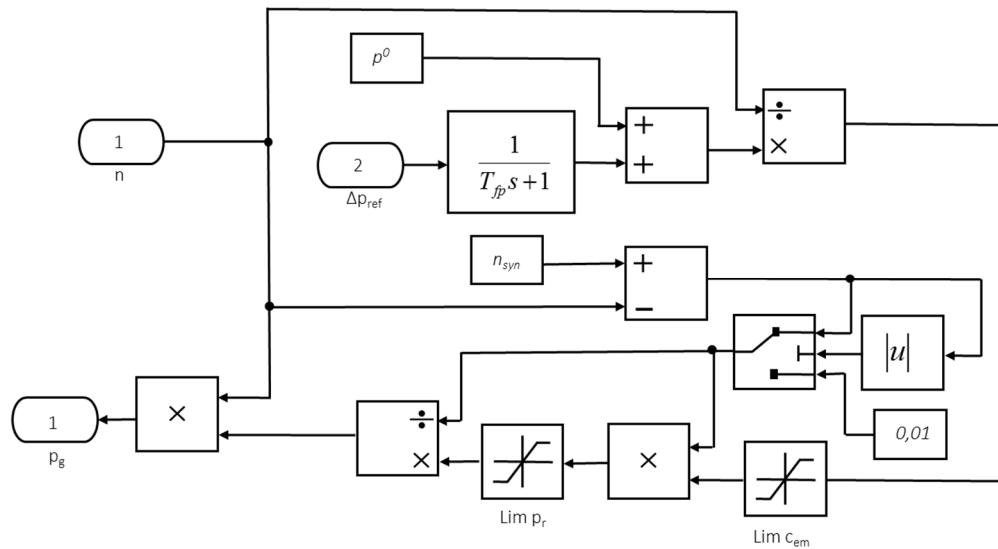

Figure 5. "DFIG electrical model" block. (T_{fp} (s) is the converter time constant and n_{syn} (p.u.) is the synchronous speed of the group). Doubly fed induction generators: DFIG.

3.8. Power System

A single node inertial model has been used in this paper to represent the isolated power system. This assumption is accepted for the time scale of the dynamics analyzed in this work [25,26]. The changes in the system frequency are calculated from the unbalance between total generation and demand in Equation (12), in the "power system" block:

$$\frac{M}{\omega^0}\frac{dF_g}{dt} = \left[\Delta p_g - \Delta p_d - D_{net}\frac{F_g}{\omega^0} + R1 + R2\right] \tag{12}$$

$$\frac{dR1}{dt} = \frac{1}{T_{net}}\left[-\frac{F_g}{\omega^0 R} - R1\right] \tag{13}$$

Wind and solar generators are supposed to be connected to the system through frequency converters and do not contribute to system inertia. The contribution of the thermal generation to the primary load-frequency control is represented by *R1* (p.u.) in Equation (13) [27]. The contribution of the thermal generation to the secondary load-frequency control *R2* (p.u.) is modelled through the transfer function proposed in [28], Figure 6. Although modern wind and solar generators could contribute to the load-frequency regulation, this contribution entails a cost: some energy will be lost [18]. Therefore, in this paper no contribution to frequency regulation from the wind and solar farms is assumed.
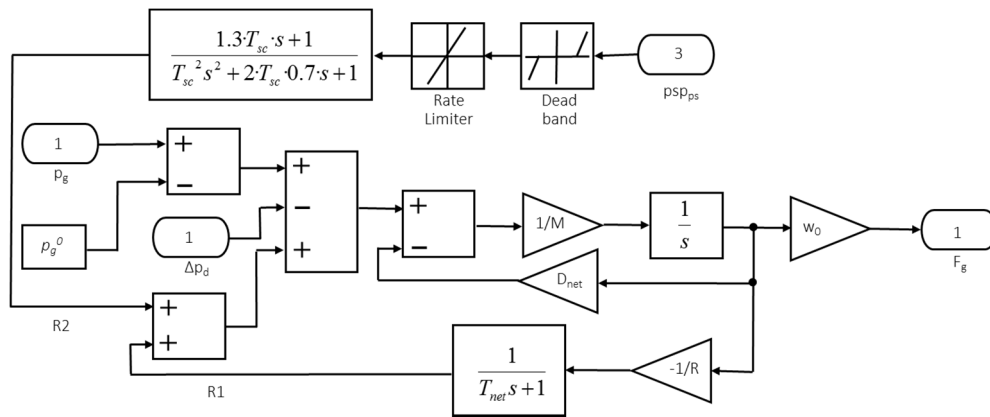
Figure 6. "Power system" block (T_{sc} (s) is the parameter of the transfer function used to model the secondary load frequency control of the synchronized thermal units).

In expressions of Equations (12) and (13), Δp_d (p.u.) is the variation in the load demand at rated frequency, Δp_g (p.u.) is the variation in the electric power delivered to grid by the PSHP, M (s) is the equivalent mechanical inertia of the power system, R (p.u.) is the equivalent permanent droop of the synchronized thermal units, D_{net} (p.u./p.u.) the power system damping constant and T_{net} (s) is the time constant of the primary load-frequency control provided by the synchronized thermal unit.

3.9. Automatic Generation Control

In the Spanish insular power systems, an AGC system is in charge of eliminating the frequency deviations after the performance of the primary load-frequency control. In this paper, the AGC system is modelled in a similar way to [7]. The proportional coefficient in the control area K_f (MW/Hz) is calculated using the recommendations of [29]. The total regulation effort RR (p.u.), is proportional to the frequency deviation F_g in Equation (14). The regulation effort is distributed among the synchronized units as a function of the participation factors K_{hp}, K_{ps}, (p.u.) in Equations (15) and (16) [30]. In expressions of Equations (15) and (16), subscript *hp* refers to the PSHP and subscript *ps* refers to the power system; psp_{hp} (p.u.) is the increment in the power set-point signal sent by the AGC, psp_{ps} (p.u.) is the increment in the power set-point of the synchronized thermal units, T_{hp} (s) is the time constant of the AGC system for the PSHP and T_{ps} (s) is the time constant of the AGC system for the synchronized thermal units:

$$RR = -K_f \frac{F_g}{\omega_0} \tag{14}$$

$$\frac{d\left(psp_{hp}\right)}{dt} = \frac{K_{hp}}{T_{hp}} RR \tag{15}$$

$$\frac{d\left(psp_{ps}\right)}{dt} = \frac{K_{ps}}{T_{ps}} RR \tag{16}$$

3.10. Model Numerical Values

In this section a summary of the main model magnitudes is presented. Table 1 contains the model base values. Table 2 lists the values of the model parameters. The parameters of the power system were properly calibrated in [7] from the system response during a load tripping event.

Table 2. Model parameter values.

Block	Parameter	Long/Short Penstock
Penstock	r	0.1363
	L	1350/300 m
	a_{p}	1000 m/s
	T_{w}	4.14/0.92 s
	T_{e}	1.35/0.30 s
Turbine-DFIG inertial model	T_{m}	6.00 s
Gross head	$h\mathrm{c}$	1.250–1.068
Speed governor	δ	2.336/0.384
	T_r	8.65/4.60 s
Electrical model doubly fed induction generator (DFIG)	T_{fp}	0.5 s
	n_{syn}	1.0 p.u.
	$c_{\mathrm{em,max}}, c_{\mathrm{em,min}}$	1.2/0.0 p.u.
	$p_{\mathrm{r,max}}, p_{\mathrm{r,min}}$	0.15/−0.15
Power control	K	0.0531 p.u.
	T_{d}	0.0191 s
	T_{fnf}	2 s
Power system	M	804 s
	R	0.0018 p.u.
	D_{net}	0.5 p.u./p.u.
	T_{net}	1 s
	T_{sc}	10 s
Automatic generation control (AGC)	T_{u}	100 s
	T_{ps}	150 s
	K_{f}	575.04 MW/Hz
	K_{u}	0.15 p.u.
	K_{ps}	0.85 p.u.

Governor PI gains have been adjusted by using two different tuning criteria. On one hand, for the long penstock configuration, the criterion proposed in [18] has been used. This criterion considers the elasticity of both water and penstock, as it is required in long penstocks [31]. On the other hand, for the short penstock configuration the tuning criterion proposed in [32] is used. This criterion is one of the most used ones for isolated power plants and usually yields moderate oscillations in the wicket gates position. As can be seen in Table 2, the head loss in the penstock, expressed in per unit values with respect to the base head, is assumed to be identical for both configurations. The possible differences that might exist between the two configurations are expected not to appreciably affect the parameters used to evaluate and compare the speed control strategies analyzed in the paper.

4. Control Strategies for the Speed Control Loop

As it was above-mentioned, different control strategies have been studied for the speed control loop of the pumped-storage unit. The studied control strategies are summarized below. It is important to mention that the option of bypassing the converter is not considered in the paper:

Strategy A ($n^{\mathrm{ref}} = n^{\mathrm{fix}}$). The reference speed n^{ref} is kept constant during the whole simulation. Two different values have been adopted: the speed ($n^{\mathrm{fix}} = 1.051$) at which the unit provides the rated power ($p_{\mathrm{g}} = p_{\mathrm{t}} = 1.0$) with the best efficiency and an intermediate gross head ($h_{\mathrm{c}} = 1.131$); and the speed ($n^{\mathrm{fix}} = 1.088$) at which the unit provides an intermediate power ($p_{\mathrm{g}} = p_{\mathrm{t}} = 0.7$) with the best efficiency and the same gross head. The first speed corresponds to the design or rated conditions, whereas the second one corresponds to an intermediate value of power that maximizes the up and down power reserve and that will likely be the most frequent steady-state operating point.

Strategy B ($n^{\mathrm{ref}} = n^{\mathrm{opt,fix}}$). The reference speed is optimum for the initial operating point (h_{c}^{0} and p^{0}) and is kept constant during the simulation.

Strategy C ($n^{\text{ref}} = n^{\text{opt,var}}$). The reference speed varies throughout the simulation as a function of the operating point (h_c and p_t). The reference speed changes every T_n seconds (hereinafter referred to as update period).

5. Simulations

The above-described strategies have been evaluated in terms of the amount of water discharged *Vol*, and the wicket gates fatigue, while providing load-frequency control, considering different initial operating points and penstock lengths, as well as different update periods for the strategy C. The wicket gates fatigue has been measured as the number of changes in the sign of the first derivative of the wicket gates position, *zvar*. Therefore, in each simulation *zvar* is an integer value but in some tables it is expressed as a decimal number resulting from the averaging of the multiple simulations. Table 3 summarizes the initial operating points considered in the simulations. The initial operating points have been superimposed on the pump-turbine hill chart in Figure 4. The dynamic response of the PSHP has been simulated with each strategy, initial operating point, and update periods for strategy C, in nine different scenarios of wind and solar power.

These scenarios have been built by combining the wind and solar photovoltaic power records presented in [33], conveniently scaled to the installed wind and photovoltaic power in the system under study. Said power records are shown in Figure 7, expressed in per unit values with respect to the maximum wind and solar power in the system analyzed in [33]. The nine scenarios are characterized in Table 4, in terms of the wind and solar power output level.

Table 3. Initial values for each operating point considered in this study. *eff* is the turbine efficiency. Superscripts 0 indicate initial conditions.

| $h_c{}^0$	p^0	$n^{\text{fix}}/n^{\text{opt,fix}}$	q^0	h^0	z^0	eff^0
		1.051	0.777	1.027	0.574	0.918
	0.8	1.088	0.781	1.027	0.587	0.912
		1.017	0.779	1.027	0.566	0.920
		1.051	0.694	1.035	0.503	0.902
1.068	0.7	1.088	0.698	1.035	0.516	0.899
		1.040	0.691	1.036	0.498	0.902
		1.051	0.601	1.044	0.428	0.881
	0.6	1.088	0.602	1.043	0.439	0.878
		1.045	0.601	1.044	0.427	0.881
		1.051	0.731	1.123	0.498	0.904
	0.8	1.088	0.722	1.123	0.501	0.903
		1.081	0.728	1.123	0.504	0.904
		1.051	0.646	1.131	0.431	0.883
1.131	0.7	1.088	0.644	1.131	0.440	0.885
		1.088	0.644	1.131	0.440	0.885
		1.051	0.562	1.137	0.364	0.859
	0.6	1.088	0.563	1.137	0.376	0.862
		1.096	0.561	1.138	0.376	0.862
		1.051	0.689	1.218	0.433	0.882
	0.8	1.088	0.684	1.218	0.440	0.886
		1.130	0.681	1.218	0.449	0.888
		1.051	0.613	1.224	0.375	0.861
1.250	0.7	1.088	0.608	1.225	0.382	0.866
		1.135	0.605	1.225	0.393	0.869
		1.051	0.536	1.230	0.317	0.835
	0.6	1.088	0.534	1.230	0.325	0.840
		1.143	0.533	1.230	0.338	0.844
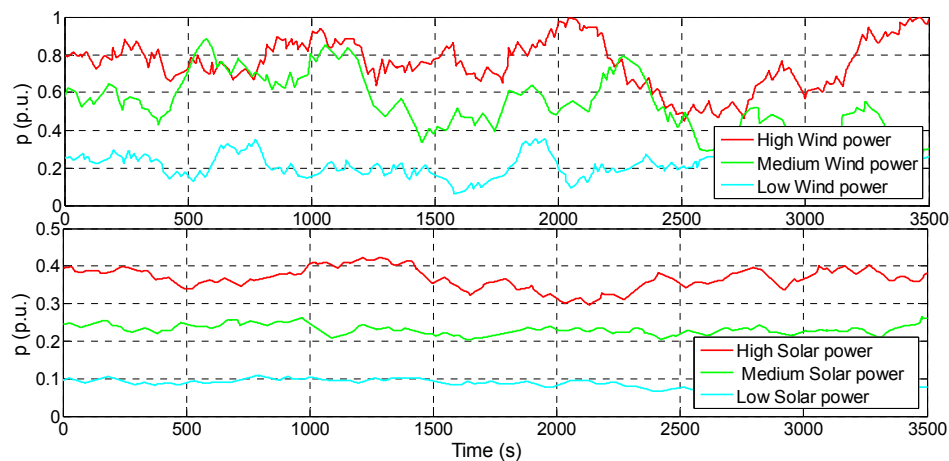
Figure 7. Wind and solar power records taken from [31].

Table 4. Wind and solar power scenarios analyzed in the paper. H = high, M = medium, L = low.

Scenario	1	2	3	4	5	6	7	8	9
Wind power output	H	H	H	M	M	M	L	L	L
Solar power output	H	M	L	H	M	L	H	M	L

6. Simulation Results

The main results obtained in this study are discussed in the following subsections. The numerical values presented in the following tables and figures are the average values across the nine considered scenarios.

6.1. Update Period

Tables 5 and 6 show the results obtained for different update periods (strategy C) and compare these results with those obtained with strategies A and B. The results corresponding to the strategy A are used as a basis for the comparison. The results included in the tables are the average values across all considered initial operation points, (p^0 = 0.6, 0.7, 0.8 and h_c^0 = 1.068, 1.131, 1.250). As can be seen in Table 5, for both long and short penstock configurations, there is an update period which minimizes *Vol* and another which minimizes *zvar*.

Table 5. *Vol* and *zvar* with the three control strategies and different update periods for the strategy C, n^{fix} = 1.0508 p.u.

Strategy		Long	Short	Long	Short
Strategy	n^{ref}	*Vol* (m^3)		*zvar*	
A	n^{fix}	23,850.1	23,920.0	80.8	113.0
Strategy	T_n-$n^{opt,var}$	ΔVol (%)		$\Delta zvar$ (%)	
	10 s	−0.2794	−0.2790	275.6	420.6
	30 s	−0.2799	−0.2791	163.9	219.4
	60 s	−0.2807	−0.2789	96.27	132.23
	120 s	−0.2815	−0.2781	46.03	73.24
C	300 s	−0.2794	−0.2740	14.20	28.42
	600 s	−0.2739	−0.2679	5.457	12.79
	900 s	−0.2753	−0.2705	2.391	8.683
	1200 s	−0.2637	−0.2593	−0.4596	3.809
	1500 s	−0.2734	−0.2706	2.140	6.857
B	$n^{opt,fix}$	−0.2620	−0.2604	−4.262	−1.533

Table 6. *Vol* and *zvar* with the three control strategies and different update periods for the strategy C, $n^{\text{fix}} = 1.0882$ p.u.

| Strategy		Long	Short	Long	Short
Strategy	n^{ref}	*Vol* (m³)		*zvar*	
A	n^{fix}	23,884.3	23,884.5	70.7	109.8
Strategy	T_n-$n^{\text{opt,var}}$	Δ*Vol* (%)		Δ*zvar* (%)	
	10 s	−0.1892	−0.2011	280.7	435.9
	30 s	−0.1898	−0.2290	176.4	227.0
	60 s	−0.1907	−0.2009	106.9	139.1
	120 s	−0.1916	−0.2001	54.09	78.30
C	300 s	−0.1896	−0.1960	21.17	32.16
	600 s	−0.1842	−0.1900	12.66	16.05
	900 s	−0.1855	−0.1926	9.277	11.83
	1200 s	−0.1736	−0.2092	6.806	6.235
	1500 s	−0.1832	−0.1926	9.484	9.947
B	$n^{\text{opt,fix}}$	−0.1715	−0.2103	2.923	0.7704

The results shown in Tables 5 and 6 confirm that the strategy C allows reducing the amount of water discharged while providing load-frequency control, with respect to the strategies A and B. However, this benefit comes at the expense of an increase in the wicket gates fatigue, especially for the short penstock configuration. The strategy B yields a reduction in the amount of water discharged of a similar magnitude to that yielded by the strategy C, with a significantly lower wicket gates fatigue.

Figures 8 and 9 show the running speed and the reference speed with the three control strategies for the long and short penstock configurations, in scenario 1 and with a specific initial operating point. By comparing Figures 8 and 9 it is observed that the lower water inertia in the short penstock facilitates the governor to maintain the unit speed close to the reference speed albeit at the expense of a considerable increase in the wicket gates fatigue, as shown in Tables 5 and 6.
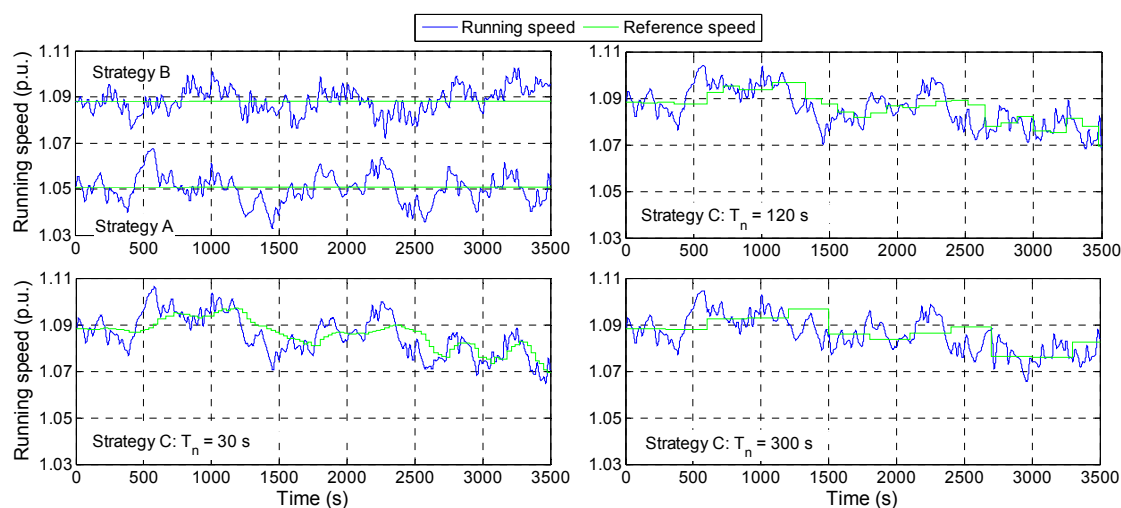
Figure 8. Running speed and reference speed with the three strategies. Long penstock configuration, $p^0 = 0.7$ p.u., $h_c{}^0 = 1.131$ p.u., scenario 1.
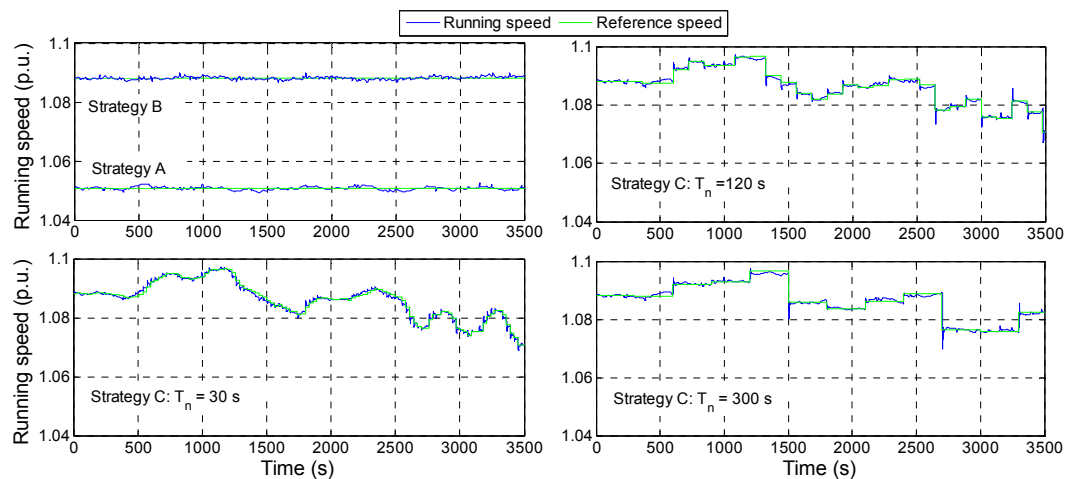
Figure 9. Running speed and reference speed with the three strategies. Short penstock configuration, $p^0 = 0.7$ p.u., $h_c^0 = 1.131$ p.u., scenario 1.

6.2. Initial Power

Tables 7 and 8 show the results obtained with the three control strategies for different initial powers delivered to the system by the PSHP. The results corresponding to the strategy A are used as a basis for the comparison. The results included in the Tables are the average values across the three initial considered gross heads. The update periods which give the least *Vol* and the least *zvar* in Tables 5 and 6 have been used for the strategy C in this case.

On the one hand, the results shown in Tables 7 and 8 confirm those discussed in Section 6.1: the strategy B yields a reduction in the amount of water discharged similar to that yielded by the strategy C, with a considerable reduction in the wicket gates fatigue. On the other hand, the results shown in these tables demonstrate that the water savings yielded by the strategies B and C slightly decrease as the initial power decreases; as can be seen in Figure 4, the efficiency barely changes with speed for the lowest initial power ($p^0 = 0.6$).

Table 7. *Vol* and *zvar* with the three control strategies, and different initial pumped storage hydropower plants (PSHP) powers p^0, $n^{fix} = 1.0508$ p.u.

p^0	Strategy	n_{ref}	Vol/zvar/ ΔVol/Δzvar	Long Penstock T_n 120/1200 s	Short Penstock T_n 30/1200 s
	A	n^{fix}	*Vol* (m³)	26,825.2	26,846.5
			zvar	78.7	119.7
0.8	B	$n^{opt,fix}$	Δ*Vol* (%)	−0.3592	−0.3554
			Δ*zvar* (%)	−3.4901	−0.6819
	C	$n^{opt,var}$	Δ*Vol* (%)	−0.3869/−0.3589	−0.3839/−0.3532
			Δ*zvar* (%)	45.51/0.1908	233.2/4.957
	A	n^{fix}	*Vol* (m³)	23,753.1	23,874.9
			zvar	89.0	113.6
0.7	B	$n^{opt.fix}$	Δ*Vol* (%)	−0.2602	−0.2601
			Δ*zvar* (%)	−3.7764	−1.986
	C	$n^{opt,var}$	Δ*Vol* (%)	−0.2794/−0.2633	−0.2769/−0.2597
			Δ*zvar* (%)	51.98/0.7453	219.8/3.265
	A	n^{fix}	*Vol* (m³)	20,972.0	21,038.6
			zvar	74.7	105.7
0.6	B	$n^{opt,fix}$	Δ*Vol* (%)	−0.1667	−0.4460
			Δ*zvar* (%)	−5.5194	−1.930
	C	$n^{opt,var}$	Δ*Vol* (%)	−0.1782/−0.1689	−0.4569/−0.4455
			Δ*zvar* (%)	40.60/−1.933	205.3/3.204

Table 8. *Vol* and *zvar* with the three control strategies, and different initial PSHP powers p^0, n^{fix} = 1.0882 p.u.

p^0	Strategy	n_{ref}	Vol/zvar/ ΔVol/Δzvar	Long Penstock T_n 120/1200 s	Short Penstock T_n 30/1200 s
0.8	A	n^{fix}	*Vol* (m³)	26,819.2	26,821.9
			zvar	70.3	115.2
	B	$n^{\text{opt,fix}}$	Δ*Vol* (%)	−0.2310	−0.3348
			Δ*zvar* (%)	7.158	1.7152
	C	$n^{\text{opt,var}}$	Δ*Vol* (%)	−0.2587/−0.2307	−0.3632/0.3326
			Δ*zvar* (%)	61.64/10.78	241.30/7.48
0.7	A	n^{fix}	*Vol* (m³)	23,870.2	23,869.2
			zvar	71.2	110.2
	B	$n^{\text{opt,fix}}$	Δ*Vol* (%)	−0.2245	−0.2319
			Δ*zvar* (%)	1.920	1.084
	C	$n^{\text{opt,var}}$	Δ*Vol* (%)	−0.2455/−0.2289	−0.2486/−0.2314
			Δ*zvar* (%)	52.17/6.13	229.92/6.50
0.6	A	n^{fix}	*Vol* (m³)	20,963.4	20,962.5
			zvar	70.6	104.1
	B	$n^{\text{opt,fix}}$	Δ*Vol* (%)	−0.0590	−0.0643
			Δ*zvar* (%)	−0.308	−0.4879
	C	$n^{\text{opt,var}}$	Δ*Vol* (%)	−0.0705/−0.0612	−0.0751/−0.0638
			Δ*zvar* (%)	48.46/3.505	209.67/4.724

6.3. Gross Head

The storage capacity of the upper reservoir is small and therefore both the water level and the gross head h_c are expected to vary frequently. Tables 9 and 10 show the results obtained with the three control strategies for different initial gross heads. The results corresponding to the strategy A are used as a basis for the comparison. The results included in the Tables are the average values across the three initial considered powers (p^0 = 0.6, 0.7 and 0.8). The update periods which give the least *Vol* and the least *zvar* in Tables 5 and 6 have been used in this case.

Table 9. *Vol* and *zvar* with the three control strategies, and different initial gross heads h_c^0, n^{fix} = 1.0508 p.u.

h_c^0	Strategy	n_{ref}	Vol/zvar/ ΔVol/Δzvar	Long Penstock T_n 120/1200 s	Short Penstock T_n 30/1200 s
1.068	A	n^{fix}	*Vol* (m³)	25,386.3	25,505.4
			zvar	68.2	112.8
	B	$n^{\text{opt,fix}}$	Δ*Vol* (%)	−0.0606	−0.0693
			Δ*zvar* (%)	6.324	2.596
	C	$n^{\text{opt,var}}$	Δ*Vol* (%)	−0.0934/−0.0618	−0.1016/−0.0668
			Δ*zvar* (%)	61.53/10.29	237.0/8.359
1.131	A	n^{fix}	*Vol* (m³)	23,790.5	23,789.6
			zvar	89.7	114.0
	B	$n^{\text{opt,fix}}$	Δ*Vol* (%)	−0.2164	−0.2185
			Δ*zvar* (%)	−4.969	−2.260
	C	$n^{\text{opt,var}}$	Δ*Vol* (%)	−0.2333/−0.2187	−0.2351/−0.2189
			Δ*zvar* (%)	49.97/−0.6262	220.8/3.145
1.250	A	n^{fix}	*Vol* (m³)	22,373.5	22,408.9
			zvar	84.5	112.3
	B	$n^{\text{opt,fix}}$	Δ*Vol* (%)	−0.5091	−0.4934
			Δ*zvar* (%)	−14.14	−4.934
	C	$n^{\text{opt,var}}$	Δ*Vol* (%)	−0.5179/−0.5106	−0.5006/−0.4923
			Δ*zvar* (%)	26.58/−11.05	200.5/−0.0772

Table 10. *Vol* and *zvar* with the three control strategies, and different initial gross heads $h_c{}^0$, $n^{\text{fix}} = 1.0882$ p.u.

$h_c{}^0$	Strategy	n_{ref}	Vol/zvar/ ΔVol/Δzvar	Long Penstock T_n 120/1200 s	Short Penstock T_n 30/1200 s
1.068	A	n^{fix}	*Vol* (m³)	25,547.1	25,547.3
			z var	65.1	110.0
	B	$n^{\text{opt,fix}}$	Δ*Vol* (%)	−0.2122	−0.2256
			Δ*zvar* (%)	11.476	5.224
	C	$n^{\text{opt,var}}$	Δ*Vol* (%)	−0.2449/−0.2134	−0.2578/−0.2231
			Δ*zvar* (%)	69.40/15.60	245.66/11.13
1.131	A	n^{fix}	*Vol* (m³)	23,740.1	23,737.8
			z var	72.1	111.0
	B	$n^{\text{opt,fix}}$	Δ*Vol* (%)	−0.0045	−0.0882
			Δ*zvar* (%)	0.628	−1.344
	C	$n^{\text{opt,var}}$	Δ*Vol* (%)	−0.0232/−0.0081	−0.1049/−0.0887
			Δ*zvar* (%)	50.17/4.671	223.75/4.111
1.250	A	n^{fix}	*Vol* (m³)	22,365.6	22,368.4
			z var	74.9	108.5
	B	$n^{\text{opt,fix}}$	Δ*Vol* (%)	−0.2978	−0.3171
			Δ*zvar* (%)	−3.333	−1.568
	C	$n^{\text{opt,var}}$	Δ*Vol* (%)	−0.3066/−0.2993	−0.3243/−0.3160
			Δ*zvar* (%)	42.70/0.149	211.48/3.46

As in the previous case, the water savings yielded by the strategies B and C are of a similar magnitude, whereas the wicket gates fatigue is notably smaller with strategy B. However, the water savings vary as a function of the initial gross head to a larger extent than as a function of the initial PSHP power. As can be seen in Table 9, the higher the initial gross head, the larger the water savings when $n^{\text{fix}} = 1.0508$ p.u. In turn, as can be seen in Table 10, when $n^{\text{fix}} = 1.088$ p.u, the further the initial gross head is from the most frequent gross head ($h_c = 1.131$ p.u.), the larger the water savings. Both results can be justified from Figure 4. As can be seen in said figure, when $n^{\text{fix}} = 1.051$, the higher the gross head (or the lower the unit speed n_{11}), the further the initial operating points are from the maximum efficiency curve, and therefore the larger the room for improving the efficiency by varying the running speed. In turn, when $n^{\text{fix}} = 1.088$ p.u, the initial operating points corresponding to the most frequent gross head (referred to as medium gross head in the figure) are very close to the maximum efficiency curve, and thus, the room for improving the efficiency by varying the running speed increases as the initial gross head separates from the most frequent gross head.

7. Conclusions

This paper analyses three different control strategies for the speed-control loop of a PSHP equipped with a pump-turbine and a DFIG when it operates in generating mode. The PSHP is connected to a small isolated power system with thermal, wind and solar generation, and which provides load-frequency control under the orders of an AGC system. The analyzed control strategies differ from each other in the way the reference speed is determined and in the frequency with which the reference speed is updated. In strategy A the reference speed is constant. Two different reference speeds have been considered for this strategy: those which maximize the efficiency for the rated operating conditions and for the most frequent operating point. In strategy B, the reference speed is constant and is optimum for the initial operating point. And in strategy C, the reference speed varies as a function of the actual operating point and is updated every T_n seconds. The control strategies have been evaluated in terms of the amount of water discharged, and the wicket gates fatigue, while providing load-frequency control. Another feasible control strategy not considered in this work would be to optimize the wicket gate fatigue instead of the efficiency or to perform a multi-objective optimization. The wicket gates fatigue has been measured as the number of changes

in the sign of the first derivative of the wicket gates position. Different T_n (update periods) have been analyzed for strategy C. For these purposes, several simulations have been performed.

The results of the simulations demonstrate that with respect to strategy A, strategies B and C allow reducing the amount of water discharged while providing load-frequency control. In general, strategy C yields higher water savings than strategy B, albeit at the expense of a significant increase in the wicket gates fatigue. Strategy B yields water savings of a similar magnitude to those yielded by strategy C, and a wicket gates fatigue lower in all cases than that of strategy C, and in most cases than that of strategy A.

The influence of the penstock length, and the initial operating point on the water usage and the wicket gates fatigue has also been analyzed. The results of the simulations show that neither the penstock length nor the initial operating point has a significant influence on the selection of the best control strategy. In general, the longer the penstock the lower the wicket gates fatigue with the three control strategies, what can be expected to a certain extent, due to the higher water inertia. The penstock length does have a considerable influence on the optimum update period for strategy C.

An interesting practical conclusion can be drawn from the results obtained in the paper. According to these results, the best way to implement variable speed in a pump-turbine unit that operates in generating mode and that provides load-frequency control, would be to update the reference speed according to the power generation schedule and keep it constant within each scheduling period (typically 1 h).

Finally, as a future line of work it would be interesting to carry out a similar study with other pump-turbines of different specific speeds. Future studies should also consider different PI tuning criteria as well as the possibility to find a trade-off solution between the hydraulic efficiency and the wicket gates fatigue by means of a multi-objective approach. Additionally, the benefits of variable speed operation from the point of view of the Transmission System Operator (TSO) should be also analyzed.

Author Contributions: José I. Sarasúa developed the simulation model blocks which correspond to the penstock and the pump-turbine unit, carried out the simulations and collaborated in the design of the control strategies and the analysis of results. Juan I. Pérez-Díaz developed the simulation model blocks which correspond to the power system and the load-frequency control, calibrated the parameters of the power system, and collaborated in the design of the control strategies and the analysis of results. Blanca Torres Vara collaborated in the development of the optimal speed block of the simulation model.

References

1. Eurelectric. *Hydro in Europe: Powering Renewables, Full Report*; the Union of the Electricity Industry—EURELECTRIC: Brussels, Belgium, 2011. Available online: http://www.eurelectric.org/media/26690/hydro_report_final-2011-160-0011-01-e.pdf (accessed on 12 December 2014).
2. Anagnostopoulos, J.; Papantonis, D. Simulation and size of a pumped-storage power plant for the recovery of wind-farms rejected energy. *Renew. Energy* **2008**, *33*, 1685–1694. [CrossRef]
3. Kaldellis, J.; Kavadias, K. Optimal wind-hydro solution for Aegean Sea islands' electricity-demand fulfilment. *Appl. Energy* **2001**, *70*, 333–354. [CrossRef]
4. Kaldellis, J.; Kavadias, K.; Christinakis, E. Evaluation of the wind-hydro energy solution for remote islands. *Energy Convers. Manag.* **2001**, *42*, 1105–1120. [CrossRef]
5. Ma, T.; Yang, H.; Lu, L.; Peng, J. Technical feasibility study on a standalone hybrid solar-wind system with pumped hydro storage for a remote island in Hong Kong. *Renew. Energy* **2014**, *69*, 7–15. [CrossRef]
6. Suul, J.A.; Uhlen, K.; Undeland, T. Wind power integration in isolated grids enabled by variable speed pumped storage hydropower plant. In Proceedings of the 2008 IEEE International Conference on Sustainable Energy Technologies (ICSET), Singapore, 24–27 November 2008.

7. Pérez-Díaz, J.I.; Sarasúa, J.I.; Wilhelmi, J.R. Contribution of a hydraulic short-circuit pumped-storage power plant to the load-frequency regulation of an isolated power system. *Int. J. Electr. Power Energy Syst.* **2014**, *62*, 199–211. [CrossRef]

8. Quintero, J.; Vittal, V.; Heydt, G.T.; Zhang, H. The impact of increased penetration of converter control-based generators on power system modes of oscillation. *IEEE Trans. Power Syst.* **2014**, *29*, 2248–2256. [CrossRef]

9. Boukhezzar, B.; Siguerdidjane, H. Nonlinear control with wind estimation of a DFIG variable speed wind turbine for power capture optimization. *Energy Convers. Manag.* **2009**, *50*, 885–892. [CrossRef]

10. Kopf, E.; Brausewetter, S. Control strategies for variable speed machines-design and optimization criteria. In Proceedings of the 2005 Hydro Conference, Villach, Austria, 17–20 October 2005.

11. Erlich, I.; Bachmann, U. Dynamic behavior of variable speed pump storage units in the German electric power system. In Proceedings of the 2002 IFAC Triennial World Congress, Barcelona, Spain, 21–26 July 2002.

12. Lung, J.-K.; Lu, Y.; Hung, W.-L.; Kao, W.-S. Modeling and dynamic simulations of doubly fed adjustable-speed pumped storage units. *IEEE Trans. Energy Convers.* **2007**, *22*, 250–258. [CrossRef]

13. Nicolet, C.; Pannatier, Y.; Kawkabani, B.; Schwery, A.; Avellan, F.; Simond, J.-J. Benefits of variable speed pumped storage units in mixed islanded power network during transient operation. In Proceedings of the 2009 Hydro Conference, Lyon, France, 26–28 October 2009.

14. Pannatier, Y.; Kawkabani, B.; Nicolet, C.; Simond, J.-J.; Schwery, A.; Allenbach, P. Investigation of control strategies for variable-speed pump-turbine units by using a simplified model of the converters. *IEEE Trans. Ind. Electr.* **2010**, *57*, 3039–3049. [CrossRef]

15. Chaudhry, M.H. *Applied Hydraulic Transients*; Van Nostrand Reinhold Inc.: New York, NY, USA, 1987.

16. Pérez-Díaz, J.I.; Wilhelmi, J.R.; Galaso, I.; Fraile-Ardanuy, J.; Sánchez, J.A.; Castañeda, O.; Sarasúa, J.I. Dynamic response of hydro power plants to load variations for providing secondary regulation reserves considering elastic water column effects. *Energy* **2012**, *1*, 159–163.

17. Sarasúa, J.; Elías, P.; Martínez-Lucas, G.; Pérez-Diaz, J.; Wilhelmi, J.; Sánchez, J. Stability analysis of a run-of-river diversion hydropower plant with surge tank and spillway in the head pond. *Sci. World J.* **2014**, *2014*. [CrossRef] [PubMed]

18. Martínez-Lucas, G.; Sarasúa, J.I.; Sánchez, J.Á.; Wilhemi, J.R. Power-frequency control of hydropower plants with long penstocks in isolated systems with wind generation. *Renew. Energy* **2015**, *83*, 245–255. [CrossRef]

19. Carravetta, A.; Fecarotta, O.; Martino, R.; Antipodi, L. Pat efficiency variation with design parameters. *Procedia Eng.* **2014**, *70*, 285–291. [CrossRef]

20. Suul, J.A.; Uhlen, K.; Undeland, T. Variable speed pumped storage hydropower for integration of wind energy in isolated grids-case description and control strategies. In Proceedings of the Nordic Workshop on Power and Industrial Electronics (NORPIE), Espoo, Finland, 9–11 June 2008.

21. Morren, J.; Pierik, J.; de Haan, S.W.H. Inertial response of variable speed wind turbines. *Electr. Power Syst. Res.* **2006**, *76*, 980–987. [CrossRef]

22. Margaris, I.D.; Papathanassiou, S.A.; Hatziargiriou, N.D.; Hansen, A.D.; Sorensen, P. Frequency control in autonomous power systems with high wind power penetration. *IEEE Trans. Sustain. Energy* **2012**, *3*, 189–199. [CrossRef]

23. Machowski, J.; Bialek, J.W.; Bumby, J.R. *Power System Dynamics: Stability and Control*, 2nd ed.; John Wiley & Sons Limited: New York, NY, USA, 2008.

24. Rodríguez, J.M.; Fernández, J.L.; Beato, D.; Iturbe, R.; Usaola, J.; Ledesma, P.; Wilhelmi, J.R. Incidence on power system dynamics of high penetration of fixed speed and doubly fed wind energy systems: Study of the Spanish case. *IEEE Trans. Power Syst.* **2002**, *17*, 1089–1095. [CrossRef]

25. Grenier, M.-E.; Lefebvre, D.; van Cutsen, T. Quasi steady-state models for long-term voltage and frequency dynamics simulation. In Proceedings of the 2005 IEEE Russia Power Tech, St. Petersburg, Russia, 27–30 June 2005; pp. 1–8.

26. Van Cutsen, T.; Grenier, M.-E.; Lefebvre, D. Combined detailed and quasi steady-state time simulations for large-disturbance analysis. *Electr. Power Energy Syst.* **2006**, *28*, 634–642. [CrossRef]

27. Mansoor, S.P.; Jones, D.I.; Bradley, D.A.; Aris, F.C.; Jones, G.R. Reproducing oscillatory behaviour of a hydroelectric power station by computer simulation. *Control Eng. Pract.* **2000**, *8*, 1261–1272. [CrossRef]

28. Egido, I.; Fernández-Bernal, F.; Rouco, L.; Porras, E.; Sáiz-Chicharro, A. Modeling of thermal generating units for automatic generation control purposes. *IEEE Trans. Control Syst. Technol.* **2004**, *12*, 205–210. [CrossRef]

29. Union for the Co-ordination of Transmission of Electricity (UCTE). Continental Europe Operation Handbook. 2004. Available online: https://www.entsoe.eu/publications/system-operations-reports/ operation-handbook (accessed on 23 December 2014).

30. Wood, A.J.; Wollenberg, B.F. *Power Generation Operation and Control*, 2nd ed.; John Wiley & Sons Limited: New York, NY, USA, 1996.

31. Clifton, L. Waterhammer and governor analysis. *Int. Water Power Dam Constr.* **1987**, *39*, 31–39.

32. Kundur, P. *Power System Stability and Control*; Balu, N.J., Lauby, M.G., Eds.; McGraw-Hill: New York, NY, USA, 1994; Volume 7.

33. Wada, K.; Yokoyama, A. Load frequency control using distributed batteries on the demand side with communication characteristics. In Proceedings of the 2012 3rd IEEE PES International Conference and Exhibition on Innovative Smart Grid Technologies (ISGT Europe), Berlin, Germany, 14–17 October 2012.